Thoracic paravertebral osteosarcoma induced by radiotherapy for esophageal cancer: A case report

BIN CHEN[1], LI ZHAO[1], LUJIAO CHEN[1], WAN SUN[2], JUN YU[3] and JIN XU[4]

[1]Department of Radiology, Shaoxing People's Hospital, Shaoxing, Zhejiang 31200, P.R. China;
[2]Department of Radiology, Zhejiang Cancer Hospital, Hangzhou, Zhejiang 310000, P.R. China;
[3]Department of Nuclear Medicine, Zhejiang University Mingzhou Hospital, Ningbo, Zhejiang 315000, P.R. China;
[4]Department of Radiology, Zhuji People's Hospital, Zhuji, Zhejiang 311800, P.R. China

Received April 16, 2025; Accepted July 30, 2025

DOI: 10.3892/ol.2025.15231

Abstract. With the wide application of radiation therapy for malignant tumors and the continuous improvement of comprehensive treatment effect, the survival period of patients has been prolonged, while the incidence of radiation-induced osteosarcoma (RIOS) has gradually increased. Compared with primary osteosarcoma, RIOS has a higher degree of malignancy and poorer prognosis, severely impacting patient survival. Currently, there are relatively few case reports on RIOS and the understanding of its imaging characteristics remains incomplete. A patient with esophageal cancer who was found to have thoracic paravertebral masses six years after receiving radiotherapy was encountered at Zhuji People's Hospital (Zhuji, China). Computed tomography (CT), magnetic resonance imaging and positron emission tomography/CT all indicated the presence of the malignant tumors. Subsequently, the patient was hospitalized for CT-guided puncture biopsy of thoracic paravertebral masses. Through multidisciplinary discussions in the departments of Medical Oncology, Orthopedics, Radiology and Pathology, a consensus was finally reached on RIOS. In conclusion, RIOS is a severe and relatively rare complication of radiotherapy with a poor prognosis. In its early stage, it is easily confused with bone changes after radiotherapy and appearance deformities after surgery. Neoplastic bone is the primary imaging feature of RIOS of esophageal cancer. By combining the patient's radiotherapy history and laboratory examinations, the diagnostic accuracy for this disease could be improved.

Correspondence to: Dr Jin Xu, Department of Radiology, Zhuji People's Hospital, 9 Jianmin Road, Taozhu Street, Zhuji, Zhejiang 311800, P.R. China
E-mail: 240482353@qq.com

Key words: radiotherapy, radiation-induced osteosarcoma, CT, MRI, PET/CT

Introduction

As one of the important treatment methods for malignant tumors, radiotherapy has provided significant survival benefits to numerous patients due to its remarkable clinical efficacy (1,2). With advancements in radiotherapy technology, patients' survival periods have gradually increased; however, ionizing radiation has also introduced serious complications. Radiotherapy plays a crucial role in the management of malignant tumors, with its primary advantage being its ability to effectively control local tumors and reduce systemic side effects (3). For example, in the treatment of skull base malignant tumors, multiple radiosurgical procedures have demonstrated high tumor control rates and progression-free survival (4). Nevertheless, despite continuous technological progress, ionizing radiation still presents certain challenges. Firstly, radiotherapy may induce radioresistance in tumors, which is associated with cancer stem cells within the tumor microenvironment. These cells can lead to tumor recurrence and metastasis post-radiotherapy (5). Additionally, internal irradiation caused by radionuclides and external irradiation from radiotherapy can damage adjacent bones and soft tissues, resulting in issues such as growth disturbances, bone marrow fibrosis, radiation-induced osteoarthritis, osteonecrosis, pathological fractures and rare malignant tumors (6,7). The incidence of radiotherapy-induced malignant tumors remains relatively low, primarily classified into carcinoma and sarcoma. Among these, carcinoma most commonly manifests as squamous cell carcinoma (8), while sarcomas are more frequently represented by osteosarcoma and fibrosarcoma (9,10). Although radiotherapy is an effective cancer treatment, one of its potential adverse effects is the induction of secondary malignant tumors. Studies indicate that squamous cell carcinoma and sarcoma are the most prevalent types of malignant tumors occurring after radiotherapy (11,12). For sarcomas, particularly osteosarcoma and fibrosarcoma, their incidence following radiotherapy is low; however, their prognosis is generally poor. Research suggests that the development of osteosarcoma post-radiotherapy correlates with the radiation dose and latency period, often manifesting many years after treatment (13). Compared to primary osteosarcoma, radiation-induced osteosarcoma (RIOS) exhibits higher malignancy and poorer prognosis,

significantly impacting patient survival. Currently, case reports on RIOS are limited (14-17) and the understanding of its imaging features remains incomplete. Radiation-induced osteosarcoma is a rare but highly aggressive complication of radiotherapy, particularly in the head and neck region. Studies have shown that the latency period for radiation-induced osteosarcoma averages 11.79 years, with a poor prognosis-72.3% of patients die within 23 months of follow-up (18). Due to its rarity and complex imaging characteristics, early diagnosis of radiation-induced osteosarcoma remains challenging (19). Non-invasive imaging modalities are crucial in diagnosing radiation-induced osteosarcoma. Techniques such as magnetic resonance imaging (MRI) and computed tomography (CT) provide detailed information on tumor distribution, tissue characteristics and invasion extent (20). Furthermore, hybrid imaging technologies like PET/CT and PET/MRI offer functional insights into tumor biology and enhance diagnostic accuracy (21). In summary, non-invasive imaging methods are vital for diagnosing radiation-induced osteosarcoma. The present study reports a rare case of radiation-induced osteosarcoma and, in conjunction with relevant literature, analyzes and discusses its imaging and clinical features.

Case report

Patients. A 64-year-old male patient who underwent gastroscopy at Zhuji People's Hospital (Zhuji, China) in February 2017 with the complaint of 'foreign body sensation while swallowing', presented with a firm mucosal swelling located 30 cm from the incisor in the mid-esophagus, raising suspicion of esophageal cancer (Fig. 1). The plain and contrast-enhanced chest computed tomography (CT) scan indicated middle thoracic esophagus occupation (Fig. 2). Subsequently, a radical surgery for esophageal cancer was performed. Postoperative pathology indicated a poorly differentiated squamous cell carcinoma of the medullary type of the esophagus, infiltrating into the fibrous tissue of the outer membrane; vascular tumor thrombi were observed and two lymph node metastases adjacent to the left recurrent laryngeal nerve, while no lymph node metastasis adjacent to the right recurrent laryngeal nerve, subcarina, azygos vein, perigastric and esophagus was detected. After excluding any contraindications for chemoradiotherapy, the patient subsequently received postoperative adjuvant radiotherapy targeting the esophageal cancer bed area, mediastinum and supraclavicular lymph node drain area: The planning target volume was 5,600 cGy/28F. Concurrently, four cycles of 'tegafur plus nedaplatin' (tegafur 1 g d1-3 + nedaplatin for injection 40 mg d1-3 + calcium levofolinate 100 mg d1-3, Q3w) were administered. Follow-up plain chest CT scan showed no significant thickening of the anastomotic tube wall and no obvious space-occupying lesions in adjacent tissues (Fig. 3). In May 2023, due to 'back discomfort', the patient underwent a plain CT scan of the thoracic vertebrae (Fig. 4) and a contrast-enhanced magnetic resonance imaging (MRI) scan of the thoracic vertebrae (Fig. 5). These investigations indicated an osteogenic mass adjacent to the right edge of the thoracic 3-5 vertebrae, suggesting malignancy. An ^{18}F-fluorodeoxyglucose (FDG)-positron emission tomography (PET)/CT scan indicated a heterogeneous dense mass shadow near the right edge of the T3-T5 vertebral bodies with increased FDG uptake (Fig. 6), suggestive of a malignant tumor. Laboratory tests showed

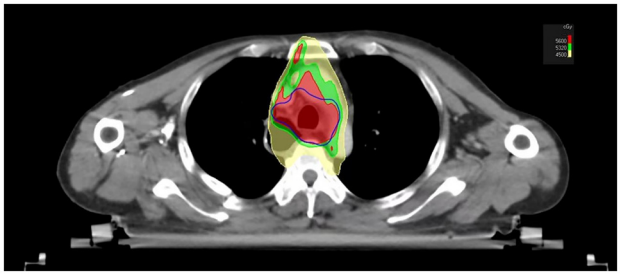

Figure 1. Target area and dose distribution map after esophageal cancer surgery. The yellow area represents the 4,500 cGy dose distribution area, which highly overlaps with the osteosarcoma area.

carbohydrate antigen 125 at 8.71 U/ml (upper limit of normal, 0-35 U/ml) and alkaline phosphatase (ALP) at 50 U/l (normal range, 40-160 U/l). The patient was subsequently admitted to the hospital and a CT-guided puncture biopsy of the thoracic paravertebral masses was performed. The pathology report (H&E staining was performed according to standard procedures) indicated the presence of anaplastic sarcoma cells and osteoid matrix produced by sarcoma cells, and tumorous bone (Fig. 7).

Immunohistochemical (IHC) method. Tissue sections, 3 μm thick, fixed in 10% neutral buffered formalin at 25˚C for 12 h, were embedded in paraffin. Staining was performed using the DAKO Autostainer Link 48 system (Agilent Technologies, Inc.). The primary antibodies, all ready-to-use reagents, were sourced from Guangzhou Anbi Ping Medical Laboratory Co., Ltd. and provided at a ready-to-use dilution, including CD34 (cat. no. IR034), ERG (cat. no. IR351), CD20 (cat. no. IPM028), paired box 5 (PAX-5) (cat. no. IR128), CD138 (cat. no. IM048), CD38 (cat. no. IM213), Kappa (cat. no. IM363), Lambda (cat. no. IM099), low molecular weight cytokeratin (CAM5.2) (cat. no. IM271), Ki67 (cat. no. IR098), P40 (cat. no. IR345), P63 (cat. no. IM383), programmed cell death ligand 1 (PD-L1) (cat. no. M3666), cytokeratin (CK) (cat. no. IM067), smooth muscle actin (SMA) (cat. no. M005), CD99 (cat. no. IR045), Vimentin (cat. no. IM142), Desmin (cat. no. IM071), S100 (cat. no. IM135), EMA (cat. no. IM074) and placental alkaline phosphatase (PLAP) (cat. no. IM131). All primary antibodies and tissue samples were incubated at 25˚C for 30 min. The secondary antibody, a ready-to-use reagent, was obtained from Agilent Technologies Singapore, utilizing the EnVision FLEX+ IHC detection system, Mouse, High pH (prediluted by the manufacturer; cat. no. K8002; Agilent Technologies, Inc.). Endogenous peroxidase activity was blocked with hydrogen peroxide blocking reagent (cat. no. SM801; DAKO; Agilent Technologies, Inc.) at 25˚C for 5 min, followed by incubation with EnVision FLEX/HRP at 25˚C for 20 min (cat. no. SM802; DAKO; Agilent Technologies, Inc.). DAB chromogen was applied at 25˚C for 5 min (cat. no. DM827; DAKO; Agilent Technologies, Inc.). The IHC test showed CD34 (-), ERG (-), CD20 (-), PAX-5 (-), CD138 (+), CD38 (-), kappa (-), lambda (-), CAM5.2 (-), BCOR (-), Ki-67 (+) 50%, p40 (-), P63 (-), PDL-1 (22C3) (-), CK (pan) (-), SMA (-), CD99 (-), Vimentin (-), Desmin (-), S-100 (-), EMA (-) and PLAP (-) (Fig. 8).

Combining the pathological and IHC findings, the diagnosis was consistent with osteosarcoma. After multidisciplinary discussions involving the departments of oncology,

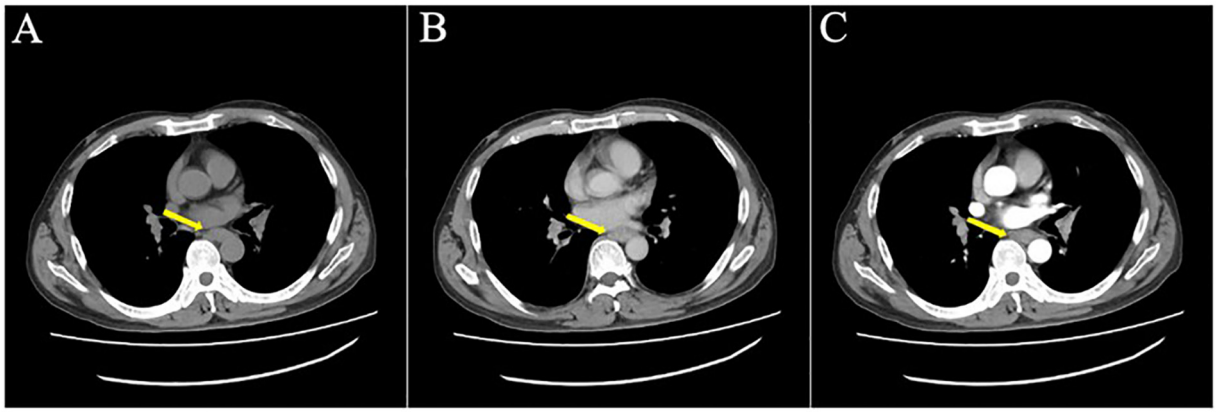

Figure 2. CT images of esophageal cancer. (A) Plain scan shows focal thickening of the middle thoracic esophagus. (B and C) Enhanced images show moderate enhancement of the middle thoracic esophagus (the yellow arrow points at the cancerous lesion). (B) Arterial phase: The lesion exhibits mild enhancement, with the degree of enhancement generally lower than that of the normal esophageal wall. (C) Venous phase: The lesion shows persistent enhancement, slightly increased compared to the arterial phase but still less than the normal esophageal wall enhancement.

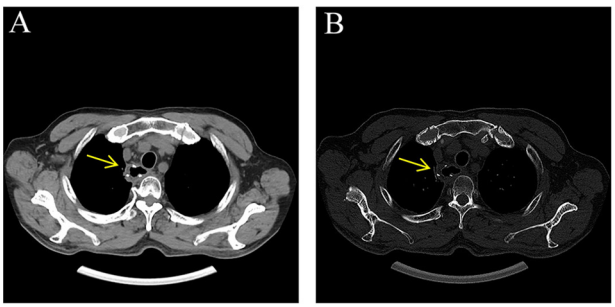

Figure 3. CT images after the surgery for esophageal cancer. (A) Mediastinal window on chest CT plain scan indicating no significant thickening of the anastomotic canal wall. (B) No obvious bone abnormalities of the thoracic vertebrae were found in the bone window (the yellow arrow indicates the anastomosis site after surgery).

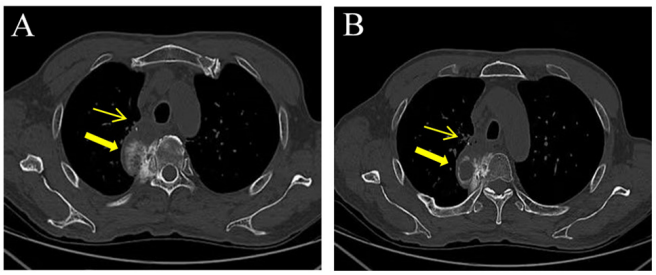

Figure 4. Postoperative CT images of esophageal carcinoma. (A) Thoracic spine CT scan shows no significant thickening of the anastomotic wall (fine arrow), with irregular dense shadows observed near the right edge of the thoracic vertebra (coarse arrow); the margins are indistinct and blurred, with patchy high-density tumor ossification visible internally. (B) Thoracic spine CT scan reveals no significant thickening of the anastomotic wall (fine arrow), with irregular dense shadows near the right edge of the thoracic vertebra (coarse arrow) and a central patchy low-density area. Sclerosis of the adjacent vertebral bodies and ribs is also present. CT, computed tomography

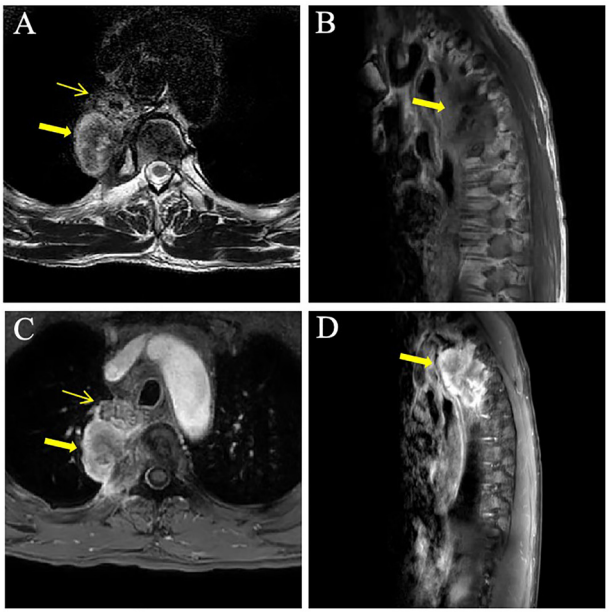

Figure 5. MR image of after esophageal cancer surgery. (A) T2WI shows that no obvious thickening of the anastomotic tube wall (thin arrow) and mass shadows (thick arrow) with patches of low signal can be seen inside. (B) T1WI shows that the lesion is located near the right margin of thoracic vertebrae 3-5 with a less equal signal. (C) Enhanced transverse view and (D) enhanced sagittal view scans demonstrate the lesion (indicated by the thick arrow) exhibiting marked heterogeneous enhancement, with the peripheral enhancement significantly more pronounced than the central area. The margins are ill-defined and the lesion involves adjacent vertebral bodies and ribs. T1WI, T1-weighted imaging.

orthopedics, radiology and pathology, based on imaging characteristics, histological examination and a history of radiotherapy, a consensus diagnosis of RIOS was reached. After multidisciplinary discussions, surgical resection of the tumor was recommended; however, the patient refused further treatment. Follow-up concluded at the end of October 2023, by which time the patient had become paraplegic and declined any additional examinations or interventions.

Discussion

RIOS mostly occurs in regions with high radiation doses. Certain studies have found that the incidence of induced osteosarcoma is proportional to the radiation dose, with total doses of 55 Gy and above increasing the risk (22,23). The radiotherapy dose reported in the present study was 56 Gy.

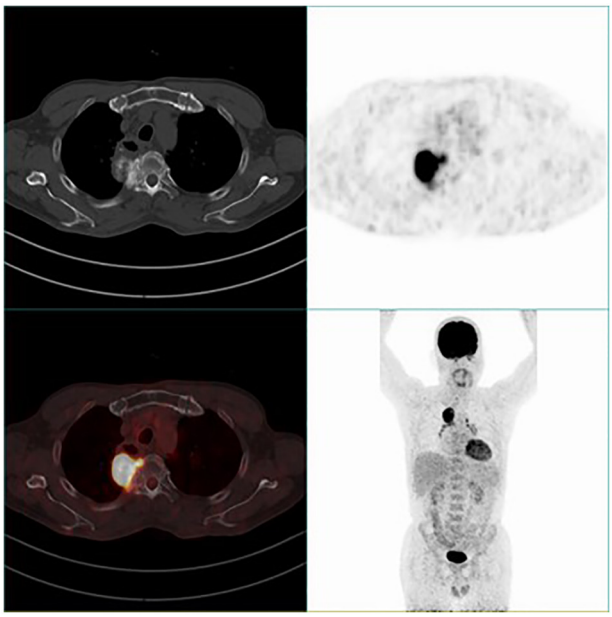

Figure 6. ^{18}F-FDG-PET/CT scan. Upper left, CT axial image demonstrating an irregular, dense lesion near the right lateral border of the thoracic vertebrae (T3-T5), measuring ~2.4x3.9x4.5 cm, with indistinct and blurred margins. Upper right, PET image showing a conspicuous irregularly shaped high FDG uptake area corresponding to the lesion seen on the CT, with SUVmax/average=14.8/9.7. Lower left, fused PET/CT image revealing complete concordance between the abnormal dense lesion on CT and the high FDG uptake region on PET. Lower right, PET Maximum Intensity Projection image displaying the distribution of FDG uptake throughout the body, with a prominent hypermetabolic lesion in the thoracic region (corresponding to T3-T5). FDG, fluorodeoxyglucose; PET, positron emission tomography; CT, computed tomography; SUV, standardized uptake value; max, maximum; avg, average.

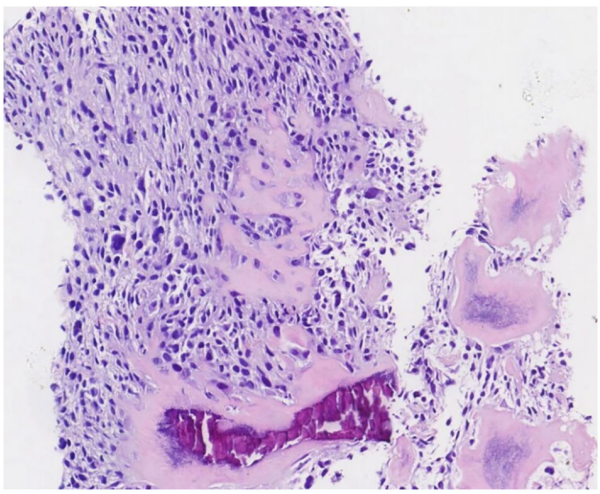

Figure 7. Puncture pathology showed that the lesion tissue contained anaplastic sarcoma cells and osteoid matrix produced by sarcoma cells. The anaplastic sarcoma cells were fusiform, round-like, with medium eosinophilic cytoplasm, obvious nuclear atypia and giant tumor cells. Eosinophilic neoplastic braided bone and osteoid matrix can be seen in the sarcoma cells and there is no osteoblast coating around it (H&E; magnification, x100).

Osteosarcoma occurring in regions with high radiation doses may also present as a second primary tumor rather than a radiation-induced tumor. Distinguishing between the two using current technologies is challenging. At present, the diagnosis of RIOS still follows the four diagnostic criteria proposed earlier by Cahan *et al* (24) and Arlen *et al* (25), which are: i) The site of the induced tumor has no evidence of malignancy prior to irradiation; ii) the induced tumor must occur within or adjacent to the radiation field; iii) the histological type of the tumor is different from that of the primary tumor; and iv) there is an incubation period of at least five years. In the present case report, there was no evidence of malignant tumor before radiotherapy. The lesion was located within the radiation field and osteosarcoma was found six years after radiotherapy, all of which conformed to the above diagnostic criteria. RIOS is classified as a rare disease, which has been reported mostly in the form of individual cases in domestic and international literatures. According to the previous literature, RIOS is a rare clinical entity considered to be a complication of radiation therapy with a poor prognosis. Its incidence rate is 0.01-0.03% of all radiation patients (26,27) and 5.5% of all osteosarcomas (27). Radiotherapy can cause adjacent bone injury, mainly including myelofibrosis, radiation-induced osteitis, osteonecrosis and pathological fracture, making early identification of osteosarcoma particularly crucial (6,7). In addition, it is still unclear whether there are differences in imaging findings between RIOS and primary osteosarcoma.

For the preparation of the present study (28,29), domestic and international literature was reviewed and the CT and MRI imaging features were summarized as follows: i) Neoplastic bone formation: This is the most characteristic imaging feature of the disease. Due to the high-density resolution of CT, the increased density of neoplastic bone can be clearly displayed, which may appear as flocculent or patchy. In pronounced cases, it can present as large ivory osteomas with considerable tumor visible even within the soft tissue mass. Therefore, CT has obvious advantages in displaying neoplastic bone and tumor cartilage calcification (particularly small neoplastic bone and calcification) compared to X-ray and MRI. On MR T1-weighted imaging (T1WI) and T2WI, neoplastic bone often appears with a low signal. Various shapes of neoplastic bone formation were observed in case reports by Kappel *et al* (30), Mahmood *et al* (31) and Venkatraman *et al* (32), as well as in the present case, with a wide range of sizes and shapes. ii) Bone destruction: On CT, this presents as osteolytic, osteoblastic or mixed bone destruction within the tumor, with the cortex exhibiting a moth-eaten appearance of bone defects. On MRI, bone destruction was indicated by low-signal bone cortex with the appearance of soft tissue signals, with partial or complete disappearance of the cortex. iii) Periosteal reaction: On CT, this can appear as acicular or radial, onion-skin periosteal reactions and the Codman triangle being rare, which may be speculated to be related to the location of the tumor. The periosteal hyperplasia showed a low signal on both T1WI and T2WI. iv) Soft tissue mass: Compared with CT, MRI has the capability of multi-sequence, multi-parameter and multi-orientation imaging, offering high tissue resolution. It is not affected by tumor osteogenesis and can comprehensively and accurately determine the extent of the tumor, commonly presenting as a low signal on T1WI and a slightly low or high signal on T2WI. After enhancement, it demonstrates significant heterogeneous enhancement with the enhancement rate of the tumor tissue edges being significantly higher than that of the central area,

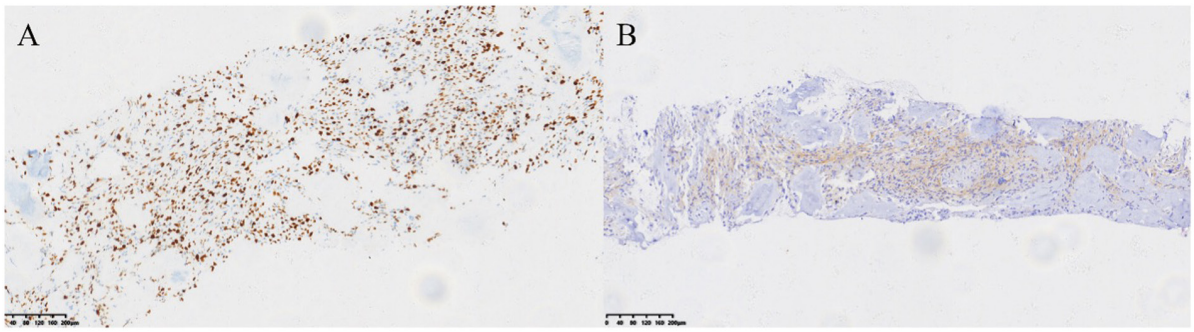

Figure 8. Immunohistochemical images: (A) Ki67 (~50% of cell nuclei are positive); (B) CD138 cell membrane positive (magnification, x100; scale bars, 200 μm).

but without specificity. ^{18}F-FDG PET/CT imaging can obtain PET, CT and fused images, providing functional, metabolic and precise anatomical structural changes, confirming each other. Since RIOS can produce different amounts of new bone-like bone tissue and is richly supplied with blood, PET/CT can not only show the characteristic neoplastic bone on CT but also show the high uptake of imaging agents. In general, a higher uptake of ^{18}F-FDG is associated with a higher malignant degree of the tumor, which can be used to evaluate the degree of malignancy of RIOS. It can also detect distant metastasis. Therefore, ^{18}F-FDG PET/CT imaging can be used for tumor staging, efficacy evaluation and monitoring of local recurrence or distant metastasis after systemic treatment (33,34). In addition, monitoring serum ALP is also an effective method to assist the diagnosis of RIOS (35,36). ALP is a glycoprotein that can accurately reflect the level of osteoblastic activity. Osteoblasts are rich in ALP and any factor that induces osteoblastic proliferation and vigorous activity can cause an increase in serum ALP activity. Therefore, a significant increase in ALP can be observed in patients with RIOS. However, no elevation of ALP was observed in the present report. In this case, ALP levels were not elevated, which diminishes the reliability of ALP as a key biomarker. Literature generally considers elevated ALP an important indicator of osteosarcoma, particularly the osteoblastic subtype, as tumor-induced bone formation releases ALP. However, a negative ALP result does not exclude RIOS and clinicians should be cautious of its potential false-negative rate when used as a diagnostic tool. The absence of ALP elevation may be due to low osteoblastic activity within the tumor, differences in tumor cell differentiation-where poorly differentiated tumors may lack ALP secretion- or individual metabolic variations and comorbidities that interfere with ALP levels. The lack of synchronous ALP elevation in this case underscores the biological heterogeneity of RIOS. While normal ALP levels do not rule out RIOS diagnosis, they highlight the limitations of relying on a single biomarker. Clinical practice should move away from overdependence on ALP and instead emphasize a combined diagnostic approach integrating imaging, clinical history and pathology. Future research should focus on elucidating the heterogeneity mechanisms of RIOS and identifying more reliable biomarkers.

The present study has certain limitations. It is based solely on a single case, lacking support from large sample sizes or multicenter data, which may restrict the generalizability of the findings. The present study focuses on diagnostic and radiological features and does not address treatment strategies or efficacy data, thus providing limited direct guidance for precise clinical management. In this case, the patient's ALP levels were not elevated, possibly due to the fact that the patient is an elderly male with a slower bone metabolic rate and inherently low baseline ALP levels, making mild elevations difficult to detect. In addition, the tumor was small and localized, likely resulting in insufficient ALP release into the bloodstream. Future studies should include a larger number of cases and more comprehensive clinical data, integrating other biomarkers and molecular biological evidence, such as genetic information, to better inform clinical treatment approaches.

In conclusion, this disease is relatively rare and easy to be misdiagnosed, which requires high attention from clinicians. Based on this case and previous literature reports, it is suggested that patients with a history of radiotherapy for malignant tumors should undergo regular imaging examinations. If a new mass appears within the radiation field, ALP is elevated and imaging exams indicate osteoblastic changes in the lesion, clinicians should consider the possibility of RIOS. PET/CT imaging can comprehensively detect the location, scope and metabolism of the lesion, and at the same time evaluate the malignancy, providing a reliable imaging basis for subsequent treatment.

Acknowledgements

Not applicable.

Funding

This study was supported by a grant from the Key Laboratory of Functional Molecular Imaging of Tumour and Interventional Diagnosis and Treatment of Shaoxing City (Shaoxing People's Hospital, Shaoxing, China; grant no. 2020ZDSYSO1).

Availability of data and materials

The data generated in the present study may be requested from the corresponding author.

Authors' contributions

BC, LZ and JX were major contributors to the conception of the study, as well as to the literature search for related studies.

BC, LZ and JX were involved in the literature review, study design and writing the manuscript. WS, JY, LC, LZ and JX were involved in the literature review, the design of the study, the critical revision of the manuscript and the processing of the figures. WS and JY confirm the authenticity of all the raw data. All authors have read and approved the final version of the manuscript.

Ethics approval and consent to participate

The study was approved by the Medical Ethics Committee of Zhuji People's Hospital (Zhuji, China; approval no. 0823).

Patient consent for publication

Written informed consent was obtained from the patient for the publication of the present case report and any accompanying images.

Competing interests

The authors declare that they have no competing interests.

References

1. Baskar R, Lee KA, Yeo R and Yeoh KW: Cancer and radiation therapy: Current advances and future directions. Int J Med Sci 9: 193-199, 2012.
2. Abshire D and Lang MK: The evolution of radiation therapy in treating cancer. Semin Oncol Nurs 34: 151-157, 2018.
3. Ozpiskin OM, Zhang L and Li JJ: Immune targets in the tumor microenvironment treated by radiotherapy. Theranostics 9: 1215-1231, 2019.
4. Coppa ND, Raper DM, Zhang Y, Collins BT, Harter KW, Gagnon GJ, Collins SP and Jean WC: Treatment of malignant tumors of the skull base with multi-session radiosurgery. J Hematol Oncol 2: 16, 2009.
5. Olivares-Urbano MA, Griñán-Lisón C, Marchal JA and Núñez MI: CSC radioresistance: A therapeutic challenge to improve radiotherapy effectiveness in cancer. Cells 9: 1651, 2020.
6. Zhang J, Qiu X, Xi K, Hu W, Pei H, Nie J, Wang Z, Ding J, Shang P, Li B and Zhou G: Therapeutic ionizing radiation induced bone loss: A review of in vivo and in vitro findings. Connect Tissue Res 59: 509-522, 2018.
7. Gladdy RA, Qin LX, Moraco N, Edgar MA, Antonescu CR, Alektiar KM, Brennan MF and Singer S: Do radiation-associated soft tissue sarcomas have the same prognosis as sporadic soft tissue sarcomas? J Clin Oncol 28: 2064-2069, 2010.
8. Wiklund TA, Blomqvist CP, Räty J, Elomaa I, Rissanen P and Miettinen M: Postirradiation sarcoma. Analysis of a nationwide cancer registry material. Cancer 68: 524-531, 1991.
9. Malone JP and Levin RJ: Second malignant tumors after treatment of nasopharyngeal carcinoma: Four case reports and literature review. Skull Base 12: 87-91, 2002.
10. Nakashima H, Takatsu T and Imai R: Radiation-induced osteosarcoma in the pubic bone after proton radiotherapy for prostate cancer: A case report. J Rural Med 17: 94-100, 2022.
11. Jiménez I, Laé M, Tanguy ML, Savignoni A, Gauthier-Villars M, Desjardins L, Cassoux N, Dendale R, Rodriguez J, Doz F, *et al*: Craniofacial second primary tumors in patients with germline retinoblastoma previously treated with external beam radiotherapy: A retrospective institutional analysis. Pediatr Blood Cancer 67: e28158, 2020.
12. de Souza LL, Pontes HAR, Santos-Silva AR, Fernandes LA, Batista LAL, Lopes MA, Khan W and Pontes FSC: Oral radiation-induced sarcomas: Systematic review. Head Neck 42: 2660-2668, 2020.
13. Wang M, Jonker B, Killen L, Bogum Y, McCormack A and Bishay RH: Fatal high-grade skull osteosarcoma 30 years following radiotherapy for Cushing's disease. Endocrinol Diabetes Metab Case Rep 2020: 20-0062, 2020.
14. Se YB, Kim DG, Park SH and Chung HT: Radiation-induced osteosarcoma after Gamma Knife surgery for vestibular schwannoma: A case report and literature review. Acta Neurochir (Wien) 159: 385-391, 2017.
15. Sugita Y, Shigemori M, Miyagi J, Ochiai S, Lee S, Watanabe T, Abe H and Morimatsu M: Radiation-induced osteosarcoma of the calvaria-case report. Neurol Med Chir (Tokyo) 32: 32-35, 1992.
16. Ulusan M, Yilmazer R, Ozluk Y, Enoz M and Suoglu Y: Radiation-induced osteosarcoma of the larynx: Case report and literature review. Ear Nose Throat J 91: E22-E25, 2012.
17. Ferreira IV, Cattan MES, Chone CT, Antolini A, Egal ESA, Altemani A and Mariano FV: Radiation-induced osteosarcoma in the head and neck region: Case report and literature review. Oral Oncol 162: 107216, 2025.
18. Zhu W, Hu F, Zhao T, Wang C and Tao Q: Clinical characteristics of radiation-induced sarcoma of the head and neck: Review of 15 cases and 323 cases in the literature. J Oral Maxillofac Surg 74: 283-291, 2016.
19. Cè M, Cellina M, Ueanukul T, Carrafiello G, Manatrakul R, Tangkittithaworn P, Jaovisidha S, Fuangfa P and Resnick D: Multimodal imaging of osteosarcoma: From first diagnosis to radiomics. Cancers (Basel) 17: 599, 2025.
20. Gennaro N, Marrari A, Renne SL, Cananzi FCM, Quagliuolo VL, Di Brina L, Scorsetti M, Pepe G, Chiti A, Santoro A, *et al*: Multimodality imaging of adult rhabdomyosarcoma: The added value of hybrid imaging. Br J Radiol 93: 20200250, 2020.
21. Amendola BE, Amendola MA, McClatchey KD and Miller CH Jr: Radiation-associated sarcoma: A review of 23 patients with post-radiation sarcoma over a 50-year period. Am J Clin Oncol 12: 411-415, 1989.
22. Tubiana M: Can we reduce the incidence of second primary malignancies occurring after radiotherapy? A critical review. Radiother Oncol 91: 4-15, 2009.
23. Mark RJ, Poen J, Tran LM, Fu YS, Selch MT and Parker RG: Postirradiation sarcomas. A single-institution study and review of the literature. Cancer 73: 2653-2662, 1994.
24. Cahan WG, Woodard HQ, Higinbotham NL, Stewart FW and Coley BL: Sarcoma arising in irradiated bone: Report of eleven cases. Cancer 82: 8-34, 1998.
25. Arlen M, Higinbotham NL, Huvos AG, Marcove RC, Miller T and Shah IC: Radiation-induced sarcoma of bone. Cancer 28: 1087-1099, 1971.
26. Goodman MA and McMaster JH: Primary osteosarcoma of the skull. Clin Orthop Relat Res 120: 110-114, 1976.
27. Salvati M, Ciappetta P and Raco A: Osteosarcomas of the skull. Clinical remarks on 19 cases. Cancer 71: 2210-2216, 1993.
28. Setiawati R, Novariyanto B, Rahardjo P, Mustokoweni S and Guglielmi G: Characteristic of apparent diffusion coefficient and time intensity curve analysis of dynamic contrast enhanced MRI in osteosarcoma histopathologic subtypes. Int J Med Sci 20: 163-171, 2023.
29. Wang CS, Yin QH, Liao JS, Lou JH, Ding XY, Zhu YB and Chen KM: Primary diaphyseal osteosarcoma in long bones: Imaging features and tumor characteristics. Eur J Radiol 81: 3397-3403, 2012.
30. Kappel AD, Bernstock JD, Ditoro DF and Lu Y: Radiation-induced intracranial osteosarcoma of the anterior skull base after treatment of esthesioneuroblastoma. BMJ Case Rep 14: e2389288, 2021.
31. Mahmood H, Hankinson P, Andrew D, Nusrath M and Khurram SA: Radiation-induced osteosarcoma involving the mandible-report of a rare diagnosis. Oral Surgery 16: 279-282, 2023.
32. Venkatraman S, Weisberg EM and Fishman EK: Radiation-induced osteosarcoma of the chest wall after treatment for unresectable thymoma. Radiol Case Rep 18: 3716-3719, 2023.
33. Toriumi K, Miyamoto H, Ikeda T and Akagi M: Radiation-induced osteosarcoma in the cervical spine after definitive radiotherapy for esophageal cancer: A case report. Spine Surg Relat Res 4: 374-376, 2020.
34. Kristenson S, Mann R, Leafblad K, Cook B and Chang J: Radiation-induced osteosarcoma following treatment of Ewing's sarcoma. Radiol Case Rep 15: 89-94, 2020.
35. Matsuda Y, Otani Y, Yasuhara T, Ando M, Higaki T, Makino T, Matsumoto H, Oyama T, Nishimori H and Date I: A case of radiation-induced osteosarcoma with RB1 gene alteration treated by skull base surgery and craniofacial reconstruction. Acta Med Okayama 77: 85-90, 2023.
36. Kappel AD, Bernstock J, Ditoro D and Lu Y: Radiation-induced intracranial osteosarcoma of the anterior skull base after treatment of esthesioneuroblastoma. BMJ Case Rep 14: e238928, 2021.